Mechanics of self-rotating double-disc grinding process

CIRP Annals - Manufacturing Technology 00 (2022) 1–4

Contents lists available at ScienceDirect

CIRP Annals - Manufacturing Technology

journal homepage: https://www.editorialmanager.com/CIRP/default.aspx

Mechanics of self-rotating double-disc grinding process

Radovan Dražumerič[a,b], Jeffrey Badger (3)[a,c], Tomas Gustavsson[d], Peter Krajnik (2)[e,*]

[a] The International Grinding Institute, San Antonio, TX, USA
[b] Faculty of Mechanical Engineering, University of Ljubljana, Ljubljana, Slovenia
[c] The Grinding Doc, San Antonio, TX, USA
[d] AB SKF, Gothenburg, Sweden
[e] Department of Industrial and Materials Science, Chalmers University of Technology, Gothenburg, Sweden

ARTICLE INFO

Article history:
Available online xxx

Keywords:
Grinding
Bearing
Double disc

ABSTRACT

Unlike most double-disc grinding processes, which use forced workpiece rotation, some double-disc processes rely on workpiece self-rotation driven by non-uniform shear forces resulting from partial wheel-workpiece coverage. This self-rotation is poorly understood, with workpiece angular frequency remaining unknown despite its importance. This paper investigates the kinematics of self-rotation via analytical modelling of the moment-equilibrium conditions, derived from experimentally determined specific-energy values. The model showed that workpiece coverage ratio is the dominant factor governing workpiece angular frequency, allowing for the choice of optimal workpiece coverage ratios that avoid (i) workpiece-stoppage and (ii) excessive frictional heat generation. The predicted velocity was validated with acoustic-emission measurements.

1. Modelling

Double-disc (DD) grinding is a high-productivity, high-accuracy process used widely in the automotive, bearing, tooling and semiconductor industries for creating parallel surfaces on two opposing flat faces [1]. Although over 100 years old, very little fundamental analysis existed on DD grinding until the 1990s. Shanbhag et al. [2] classified DD grinding into three types: (i) linear through-feed; (ii) rotary through-feed; and (iii) oscillating, using a reciprocating swing arm. In all three of these operations, the workpiece traverses through the opposing wheels. Rotation of the workpiece is "free" in that it may or may not rotate depending on the moment acting on the workpiece. However, rotation is not integral to the process and a lack of rotation is typically not detrimental to workpiece quality. Similarly, free workpiece rotation also occurs in DD grinding with planetary kinematics [3]. Here, the workpiece is held within a carrier and the kinematics resembles that of lapping [4].

In addition, there is another type of double-disc grinding where the workpiece is held within a fixed, non-traversing bushing of an index carrier (Fig. 1), allowing for workpiece rotation while two wheels are simultaneously plunged axially into the workpiece. The unique aspect of this type of DD grinding is that the workpiece faces are not fully covered by the wheel. This results in non-uniform grinding shear forces on the workpiece and, consequently, a moment acting to force the workpiece to self-rotate within the bushing. The angular frequency of this rotation is of vital importance. If it is too high, the frictional forces at the bushing-workpiece interface cause excessive heat generation, resulting in thermal damage to the bushing and possible cracking. In contrast, if the workpiece rotational speed is too low, the workpiece runs the risk of stopping, resulting in a step being ground into the workpiece, causing it to be scrapped.

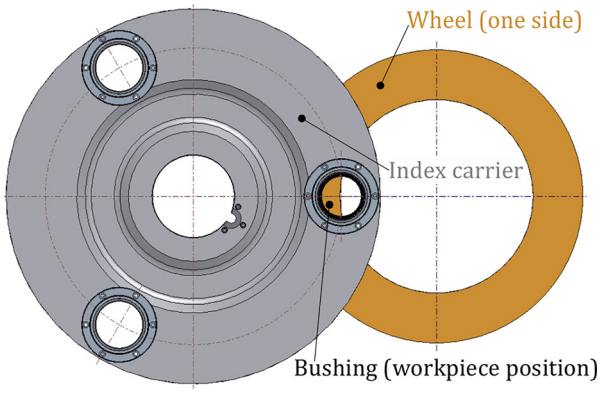

Fig. 1. Schematic of index-carrier setup for double-disc grinding.

Aside from a proprietary numerical simulation developed by the Swedish bearing manufacturing company SKF, to the authors' knowledge little has been written about this important process. To gain a fundamental understanding of the mechanics of the workpiece self-rotation, an analytical model of process geometry and kinematics was developed. The moment equilibrium was solved to predict the workpiece angular frequency.

* Corresponding author.
E-mail address: krajnik@chalmers.se (P. Krajnik).

https://doi.org/10.1016/j.cirp.2022.03.033

Monitoring of the workpiece angular frequency using acoustic emission (AE) was also investigated. While AE is an established method for monitoring grinding and dressing processes [1, 5, 6], no solutions are available for monitoring the rotation of a workpiece in a bushing. Therefore, the challenges associated with measuring the steady-state workpiece angular frequency are considered. Process details were taken from SKF and experimental data was collected to obtain the characteristic specific-energy curve and to validate the model of process mechanics. Recommendations are given for choosing workpiece coverage ratios that ensure viable workpiece rotational speeds.

2. Modelling

The most influential input parameter in the process geometry is the workpiece coverage ratio, *WCR*, expressed as:

$$WCR = \frac{\Delta_0 + r_w}{2r_w}, \tag{1}$$

where Δ_0 is the workpiece-centre position with respect to the grinding wheel radius, r_s, and r_w is the workpiece radius (Fig. 2a). At $WCR = 0$ there is zero coverage (no wheel-workpiece contact); at $WCR = 1$ there is full coverage (the entire workpiece is in contact with the wheel). At high *WCR*s, the workpiece angular frequency, ω_w, is lower, resulting in a higher risk of workpiece stoppage. At low *WCR*s, the workpiece angular frequency is high, resulting in greater frictional heat generation at the workpiece-bushing interface and greater bushing wear. Any process control involving a rotating workpiece, be it forced-driven or self-rotating, requires knowing the angular frequency. Therefore, the angular frequency is the primary modelling output here.

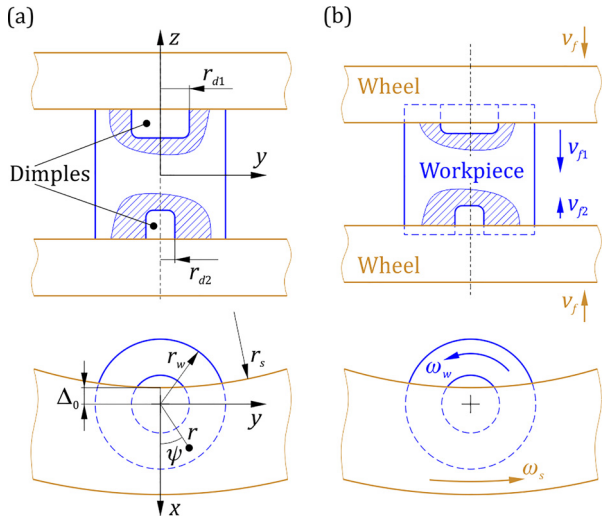

Fig. 2. Geometry (a) and kinematics (b) of double-disc grinding process.

The workpiece is restricted only in the radial direction (by the bushing). It can move freely within the bushing in the axial direction. The fixed plunge feedrate, v_f, of the closing of the wheels will result in two different feedrates, v_{f1} and v_{f2}, owing to the dissimilar axial forces caused by the dissimilar geometries on the opposing workpiece faces (Fig. 2b). This dissimilarity is the different dimples radii (r_{d1} and r_{d2}), as is the case of cylindrical rolling elements for bearings. In practice, v_f can be programmed for each wheel individually, but this does not affect the modelling approach.

The fundamental law governing the process kinematics can be expressed in terms of moment equilibrium for each workpiece face and the associated feedrate distribution:

$$\begin{aligned} &M_w(\omega_w, v_{f1}) = \mu r_w F_t(\omega_w, v_{f1}),\\ &M_w(\omega_w, v_{f2}) = \mu r_w F_t(\omega_w, v_{f2}), \quad \Rightarrow \boldsymbol{\omega_w, v_{f1}, v_{f2}}\\ &v_f = (v_{f1} + v_{f2})/2, \end{aligned} \tag{2}$$

where M_w is the moment on the workpiece face, $F_t = |\vec{F}_t|$ is the summation of tangential grinding force vectors acting also on the bushing, and μ is the coefficient of friction at the workpiece-bushing interface. Note that the moment and the tangential force depend on ω_w and the particular feedrate (v_{f1} or v_{f2}).

The moment M_w is obtained by integrating contributions of dM_w over the contact surface S_c:

$$M_w = \int\int_{S_c} \frac{dM_w}{dS_c} dS, \tag{3}$$

where the derivative dM_w/dS_c, is the workpiece moment per unit area, calculated as an axial projection of the cross product of workpiece radius vector $\vec{r}$ and shear vector $\vec{\tau} = d\vec{F}_t/dS_c$:

$$\frac{dM_w}{dS_c} = (\vec{r} \times \vec{\tau}) \cdot \vec{e}_z. \tag{4}$$

Here, the contact surface is comprised primarily of the workpiece-face portion, S_{face}, and the minor side-plunge portion, S_{plunge}, according to: $S_c = S_{face} + S_{plunge}$. An illustration of the workpiece-moment distribution is shown in Fig. 3. The integration of $d\vec{F}_t$ over the contact surface S_c gives the tangential-force vector:

$$\vec{F}_t = \int\int_{S_c} \frac{d\vec{F}_t}{dS_c} dS. \tag{5}$$

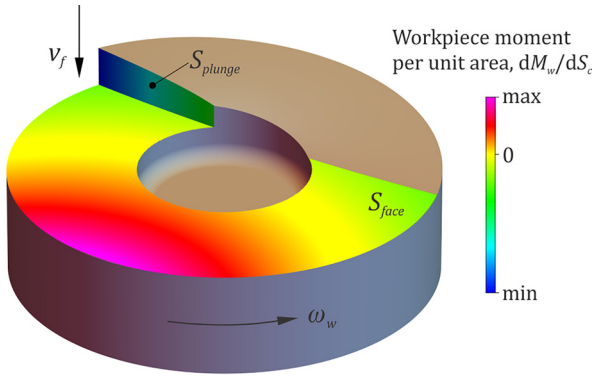

Fig. 3. Illustration of workpiece-moment distribution on wheel-workpiece contact surface.

Following first principles in the theory of aggressiveness [7], the magnitude of the shear vector depends on the specific grinding energy, e, and the point aggressiveness, $Aggr^*$, according to:

$$\vec{\tau} = -\frac{\vec{v}}{|\vec{v}|} e \cdot Aggr^*. \tag{6}$$

The modelling perspective was chosen considering movement of the workpiece relative to a "fixed" grinding wheel. Therefore, the direction of the shear vector $\vec{\tau}$ in a contact point is opposite to the direction of the relative velocity vector $\vec{v}$.

The process kinematics requires the relative-velocity vector for each workpiece face in polar coordinates (r, ψ) via the feedrate variable $v_{f1,2}$, according to:

$$\vec{v}\ (r, \psi) = \left[(\omega_s - \omega_w) r \sin\psi, -\omega_s d_{ws} - (\omega_s - \omega_w) r \cos\psi, v_{f1,2}\right], \tag{7}$$

where ω_s is the wheel angular frequency, and d_{ws} is the distance between the wheel and the workpiece centers, determined using the workpiece coverage ratio (Eq. (1)):

$$d_{ws} = r_s + \Delta_0 = r_s + r_w(2WCR - 1). \tag{8}$$

The material removal takes place on the face of the grinding wheel as well as on the side-plunge portion of the wheel. The $Aggr^*$ associated with these two portions are very different: (i) $Aggr^*_{face}$ is acting over a large surface area, whereas (ii) $Aggr^*_{plunge}$ is concentrated in a very small contact area. In general, $Aggr^*_{plunge} \gg Aggr^*_{face}$. The point aggressiveness is calculated according to the fundamental definition, i.e., $Aggr^* = \vec{v} \cdot \vec{n} / \sqrt{\vec{v} \cdot \vec{v} - (\vec{v} \cdot \vec{n})^2} \approx \vec{v} \cdot \vec{n} / |\vec{v}|$ [7], where $\vec{n}$ is the wheel-surface normal. This necessitates determination of the wheel

Please cite this article as: R. Dražumerič et al., Mechanics of self-rotating double-disc grinding process, CIRP Annals - Manufacturing Technology (2022), https://doi.org/10.1016/j.cirp.2022.03.033

geometry via a normal vector, calculated for the face and side-plunge portion as:

$$\vec{n}_{face} = (0,0,1),$$
$$\vec{n}_{plunge}(r) = \frac{(d_{ws} + r\cos\psi_{\max}(r), r\sin\psi_{\max}(r), 0)}{\sqrt{d_{ws}^2 + r^2 + 2rd_{ws}\cos\psi_{\max}(r)}}. \quad (9)$$

The specific grinding energy is correlated with $Aggr^*$ as:

$$e = e_0 + \frac{\tau_0}{Aggr^*}, \quad (10)$$

which gives the magnitude of the shear vector $\tau = |\vec{\tau}|$ (Eq. (6)), calculated as:

$$\tau = e_0 Aggr^* + \tau_0. \quad (11)$$

Here, τ_0 corresponds to $\tau(Aggr^* = 0)$, while e_0 relates to $e(Aggr^* \to \infty)$.

3. Experimental

Experiments were performed to: (i) determine the model parameters, and (ii) validate the workpiece angular frequency.

A Lidköping DG300 double-disc face-grinding machine was used to grind 100CrMnSi6-4 bearing-steel cylindrical rollers with two resin-bonded Al_2O_3 grinding wheels (90-mesh, diameter 300 mm) using a 4.5%-concentration emulsion coolant. The grinding power was measured in both spindles via the spindle IPO-trace function of the Siemens Sinumerik 840D controller.

Two workpiece geometries were considered: Roller A ($r_w = 15$ mm, $r_{d1} = 1.5$ mm, $r_{d2} = 6$ mm) positioned at $WCR = 0.65$, to determine the specific-energy curve (Fig. 4); and Roller B ($r_w = 15$ mm, $r_{d1} = 8.5$ mm, $r_{d2} = 6$ mm), positioned at $WCR = 0.7$, to measure the workpiece angular frequency.

The speed of the wheels was a constant 1080 RPM (17 m/s). Dressing was performed using a multipoint blade dresser (four 0.8-mm-wide mono-crystalline diamonds) with a dressing depth $a_d = 0.018$ mm and an overlap ratio $U_d = 1.5$.

In DD grinding, three major types of AE sources are present: (i) machine background noise, (ii) wheel-workpiece grinding action (rubbing, cutting and plowing), and (iii) frictional contact between the bushing and the workpiece. AE energy was detected by a Dittel 4100–2 process-monitoring system using a Mini-S sensor mounted on the index carrier. This mounting position proved superior for obtaining a high signal-to-noise ratio for the bushing/workpiece contact in comparison to having the sensor attached to the grinding spindle. A Fast Fourier Transform (FFT) was performed on the raw signal during the steady-state portion of the grinding cycle. Sampling for the FFT was done at 30 kHz.

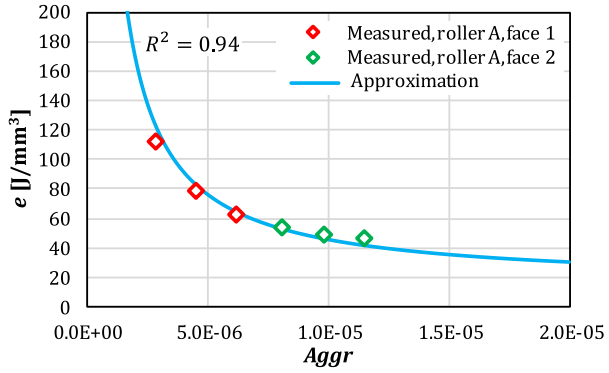

Fig. 4. Specific energy curve.

3.1. Parameter identification

The model describing process mechanics contain three unknown parameters which need to be experimentally determined: μ, e_0, and τ_0. The grinding power was measured for three different feedrates, $v_{f,i} = 48,\ 64,\ 80\ \mu$m/s, for each wheel individually (i.e. $P_{s1,i}$ and $P_{s2,i}$). The parameter identification involves the following relationships for the specific-energy data points:

$$e_{1,i} = e_0 + \frac{\tau_0}{Aggr(\omega_{w,i}, v_{f1,i})} = \frac{P_{s1,i}}{Q_w(v_{f1,i})},$$
$$e_{2,i} = e_0 + \frac{\tau_0}{Aggr(\omega_{w,i}, v_{f2,i})} = \frac{P_{s2,i}}{Q_w(v_{f2,i})}, \quad (12)$$

where, material removal rate is determined as:

$$Q_w = \int\int_{S_c} \vec{v}\cdot\vec{n}\ \mathrm{d}S = \pi\left(r_w^2 - r_{d1,2}^2\right)v_{f1,2}, \quad (13)$$

and the aggressiveness number is calculated according to [7]:

$$Aggr = \int\int_{S_c} Aggr^* \mathrm{d}S/S_c = \int\int_{S_c} \frac{\vec{v}\cdot\vec{n}}{|\vec{v}|}\mathrm{d}S/S_c. \quad (14)$$

The key challenge in parameter identification is that process kinematics depends on the unknown parameters, i.e. $\omega_{w,i} = \omega_{w,i}(\mu, e_0, \tau_0)$, $v_{f1,i} = v_{f1,i}(\mu, e_0, \tau_0)$, $v_{f2,i} = v_{f2,i}(\mu, e_0, \tau_0)$. This leads to a nonlinear least-square regression problem for the specific-energy curve, $e = e_0 + \tau_0/Aggr$, to fit the data points $(Aggr_{1,i}, e_{1,i})$ and $(Aggr_{2,i}, e_{2,i})$ which also depend on the three unknown parameters. The solution of the problem gives the following values: $\mu = 0.17$, $e_0 = 15$ J/mm^3, and $\tau_0 = 0.305$ MPa. The resulting data points based on the measured grinding power with the corresponding specific-energy curve are shown in Fig. 4. Here, larger values of e are associated with face 1 grinding due to the larger grinding surface ($r_{d1} < r_{d2} \Rightarrow v_{f1} < v_{f2}$).

3.2. Workpiece angular frequency validation

Direct measurement of workpiece angular frequency is challenging due to the isolation of the workpiece within the bushing and the possibility that any measurement technique involving physical contact with the workpiece may itself affect the rotational speed. One indirect, non-contact possibility is detecting AE signal of the index carrier, which was investigated here.

Fig. 5 shows the FFT results for three different measurements when grinding Roller B with $WCR = 0.7$ and $v_f = 64\ \mu m/s$. The dominant frequencies correspond to 55.5, 42 and 48.9 Hz, which is close to the predicted value of 49 Hz ($\omega_w = 307.9$ rad/s).

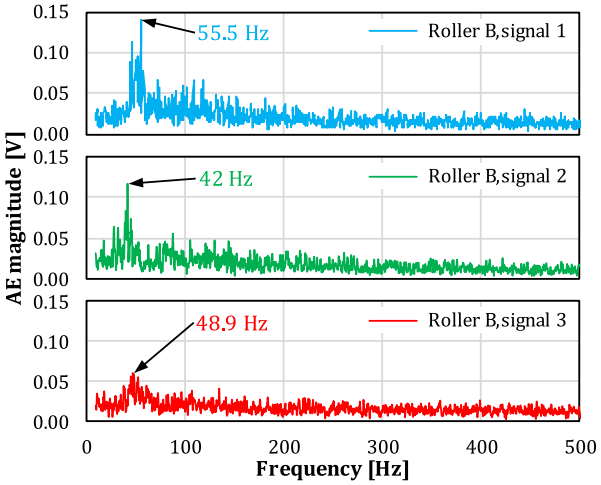

Fig. 5. Workpiece rotational frequency measurements.

4. Simulation

The validated model enables the simulation of key process outputs. Fig. 6 shows how the total material removal rate is divided between the wheel face and the side-plunge portion of the wheel.

Please cite this article as: R. Dražumerič et al., Mechanics of self-rotating double-disc grinding process, CIRP Annals - Manufacturing Technology (2022), https://doi.org/10.1016/j.cirp.2022.03.033

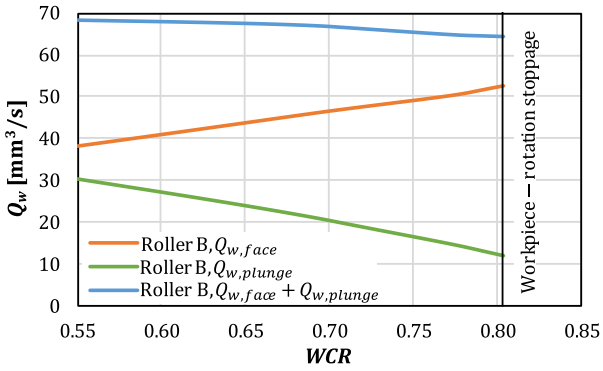

Fig. 6. Material removal rate vs. workpiece coverage ratio (Roller B).

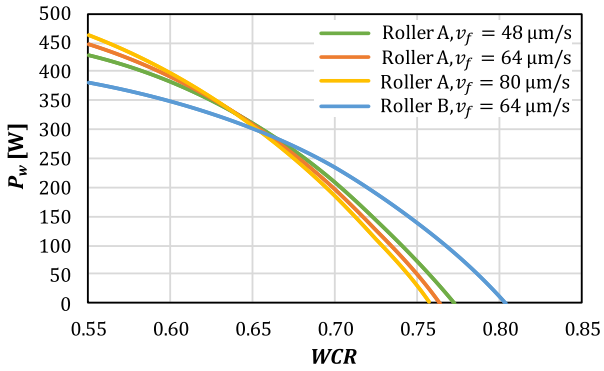

Fig. 9. Workpiece power vs. workpiece coverage ratio.

While the total material removal rate might be expected to be independent of *WCR*, this is not strictly true owing to the different feedrates because of the different dimple sizes. For example, at *WCR* ∼ 0.5, the material removal is divided equally between the face of the wheel and its side-plunge portion. However, as *WCR* increases, material removal on the face becomes more dominant.

The predicted workpiece angular frequency depends on *WCR*, feedrate and workpiece geometry. For all cases, the increase in *WCR* and v_f causes the reduction of workpiece angular frequency until the workpiece rotation halts (Fig. 7). Workpiece rotation also depends on the dimple size. For example, a workpiece without geometrical features (full face) rotates slower in comparison to a ring-like workpiece. The measured angular frequency based on AE signals for Roller B is included in Fig. 7 via its average value and standard deviation.

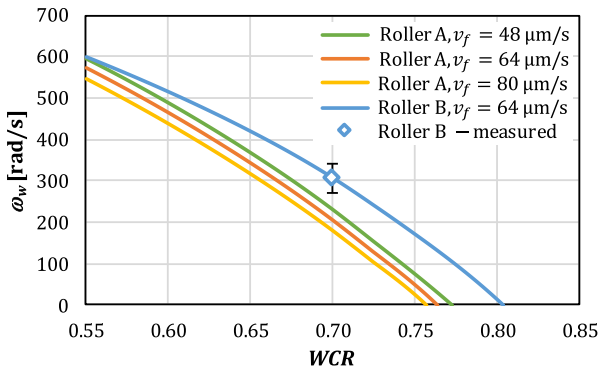

Fig. 7. Workpiece angular frequency vs. workpiece coverage ratio.

In contrast to workpiece rotation, an increase in *WCR* and v_f leads to a higher workpiece moment M_w as in Fig. 8. Similarly, a full-faced (no dimple) workpiece increases M_w. Therefore, it is important to simulate the overall effect of *WCR* via workpiece power, $P_w = M_w\omega_w$. This power corresponds to frictional power at the workpiece-bushing contact.

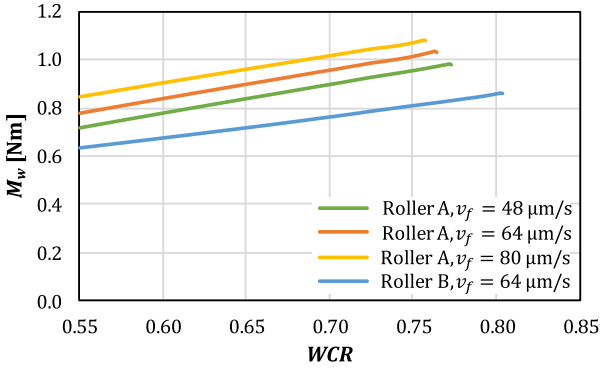

Fig. 8. Workpiece moment vs. workpiece coverage ratio.

Fig. 9. shows that power decreases with increasing *WCR*. As mentioned earlier, low *WCR*s should be avoided to reduce heat generation in the bushing. In this respect, increasing *WCR* is beneficial. However, the workpiece-stoppage threshold must be quantified and avoided. For the illustrated case study, a safe setup would be around *WCR* = 0.65. Here, the bushing heating is not excessive and the process runs far from the workpiece stoppage threshold, yielding a robust grinding operation.

5. Conclusions

An investigation was made into the mechanics of self-rotating, partial-contact double-disc grinding. An analytical model of the geometry and kinematics was developed to quantify the grinding shear forces that produce workpiece rotation. The model showed that the workpiece coverage ratio was the most influential input and could be optimally chosen to avoid workpiece stoppage on one hand and excessive workpiece-bushing heat generation and bushing wear on the other. Acoustic emission detection was used to indirectly identify workpiece rotation and validate the model.

Declaration of Competing Interest

The authors declare that they have no known competing financial interests or personal relationships that could have appeared to influence the work reported in this paper.

Acknowledgments

This research was self-funded by the International Grinding Institute (IGI) and AB SKF. The authors thank Henrik Ekblad of UVA Lidköping for contributing to this work. The project was carried out under the umbrella of the IGC competence network belonging to Chalmers Centre for Metal Cutting Research (MCR).

References

[1] Marinescu ID, Hitchiner M, Uhlmann E, Rowe WB, Inasaki I (2007) *Handbook of Machining with Grinding Wheels*, CRC Press.
[2] Shanbhag N, Rajan M, Manjunathaiah J, Krishnamurty S, Malkin S (1998) Analysis and simulation of double disc grinding. *Trans. NAMRI/SME* 26:111–116. Atlanta.
[3] Uhlmann E, Hoghé T, Kleinschnitker M (2013) Grinding wheel wear prediction at double face grinding with planetary kinematics using analytic simulation. *Int. J. Adv. Manuf. Technol.* 69:2315–2321.
[4] Uhlmann E, Ardelt T, Spur G (1999) Influence of kinematics on the face grinding process on lapping machines. *Ann. CIRP* 48(1):281–284.
[5] Inasaki I, Okamura K (1985) Monitoring of dressing and grinding processes with acoustic emission signals. *Ann. CIRP* 34(1):277–280.
[6] Karpuschewski B, Wehmeier M, Inasaki I (2000) Grinding monitoring system based on power and acoustic emission sensors. *Annals of the CIRP* 49(1):235–240.
[7] Dražumerič R, Badger J, Roininen R, Krajnik P (2020) On geometry and kinematics of abrasive processes: the theory of aggressiveness. *Int. J. Mach. Tools Manuf.* 154:103567.

Please cite this article as: R. Dražumerič et al., Mechanics of self-rotating double-disc grinding process, CIRP Annals - Manufacturing Technology (2022), https://doi.org/10.1016/j.cirp.2022.03.033